

Application of Photoelectron Spectromicroscopy to a Systematic Study of Toxic and Natural Elements in Neurons

Gelsomina De Stasio,^{a,b} D. Dunham,^{c,d} B. P. Tonner,^{c,d} Delio Mercanti,^e
M. Teresa Ciotti,^e Paolo Perfetti^b and G. Margaritondo^a

^a*Institut de Physique Appliquée, Ecole Polytechnique Fédérale, PH-Ecublens, CH-1015 Lausanne, Switzerland,* ^b*Istituto di Struttura della Materia del CNR, Via Enrico Fermi 38, Frascati, Roma, Italy,* ^c*Department of Physics, University of Wisconsin–Milwaukee, Milwaukee, Wisconsin 53211, USA,* ^d*Synchrotron Radiation Center, University of Wisconsin, Madison, Wisconsin 53706, USA,* and ^e*Istituto di Neurobiologia del Consiglio Nazionale delle Ricerche, Viale Marx 15, 00137 Roma, Italy*

(Received 21 October 1994; accepted 4 November 1994)

A systematic photoelectron spectromicroscopy study is presented of the spatial distribution of a toxic element, aluminium, iron or chromium, in neuron cultures, after exposure to a solution of the element. The study was performed by the X-ray secondary-emission microscopy (XSEM) version of photoelectron spectromicroscopy. The distribution of the elements was investigated with two complementary approaches: digital subtraction imaging and individual X-ray absorption spectra from microscopic areas. The results coherently indicate different localization patterns for different elements, and, in particular, extreme localization of aluminium to a few rare cells identifiable as Purkinje neurons. In the case of iron-exposed specimens, the distribution analysis was extended to naturally present phosphorus, and used to estimate the XSEM sensitivity.

Keywords: photoemission; microscopy; element mapping; XSEM; neurons.

1. Introduction

We performed systematic microchemical analysis of a number of cerebellar granule cell cultures after exposure to aluminium, chromium or iron solutions. The experiments are the first systematic application of the new experimental technique of synchrotron radiation photoelectron spectromicroscopy to toxicology problems (De Stasio, Koranda *et al.*, 1992; De Stasio, Perfetti *et al.*, 1992; De Stasio, Dunham *et al.*, 1993; De Stasio, Hardcastle *et al.*, 1993; De Stasio, Perfetti *et al.*, 1993; Margaritondo & Cerrina, 1990; Margaritondo, 1992). The approach, based on X-ray secondary-emission microscopy (XSEM) (Tonner & Harp, 1988; Koranda & Zhang, 1992), was capable of revealing the spatial distribution of toxic and non-toxic elements, with a resolution of the order of 0.5 μm or better. A complete comparison between XSEM spectromicroscopy and other established methods of determining trace-element distribution in cells is described by De Stasio, Cerrina, Tonner, Mercanti & Margaritondo (1994).

We found evidence of aluminium localization to a very few cells, apparently of the same type. From approximately 10^5 investigated cells of the aluminium-exposed cultures, aluminium was found in only three which appear to have the morphology of Purkinje neurons (Cohen-Cory, Dreyfus & Black, 1991).

Similar studies of the iron distribution revealed the metal spread throughout the specimens, and not confined as is the

aluminium to structures of specific types of cells. In the case of chromium-exposed specimens, the element was found to be localized to specimen areas whose size was less than $\sim 20 \mu\text{m}$, but again without being confined to specific neurons like aluminium, or to biological structures. Finally, the analysis was extended in one case to the detection of physiologically present phosphorus.

2. Experimental procedures

2.1. Photoelectron spectromicroscopy

The core part of the present study is based on the recently developed technique of photoelectron spectromicroscopy (De Stasio, Koranda *et al.*, 1992; De Stasio, Perfetti *et al.*, 1992; De Stasio, Dunham *et al.*, 1993; De Stasio, Hardcastle *et al.*, 1993; De Stasio, Perfetti *et al.*, 1993; Margaritondo & Cerrina, 1990; Margaritondo, 1992; Tonner & Harp, 1988; Koranda & Zhang, 1992). In a conventional photoemission experiment (Margaritondo, 1988), photoelectrons emitted by a macroscopic portion of a specimen are analyzed to obtain information on a variety of properties. The non-microscopic nature of these experiments is not the choice of the experimentalist, but a consequence of the low signal level in a typical photoemission experiment.

Recent instrumentation advances (De Stasio, Koranda *et al.*, 1992; De Stasio, Perfetti *et al.*, 1992; De Stasio, Dunham *et al.*, 1993; De Stasio, Hardcastle *et al.*, 1993; De Stasio, Perfetti *et al.*, 1993; Margaritondo & Cerrina, 1990;

Margaritondo, 1992; Tonner & Harp, 1988; Koranda & Zhang, 1992) have made it possible to overcome this obstacle and to perform photoemission experiments in a submicrometer range of lateral resolution. This approach was rapidly extended to biological specimens for preliminary feasibility tests (De Stasio *et al.*, 1990, 1991; De Stasio, Koranda *et al.*, 1992; De Stasio, Perfetti *et al.*, 1992; De Stasio, Dunham *et al.*, 1993; De Stasio, Hardcastle *et al.*, 1993; De Stasio, Perfetti *et al.*, 1993; Margaritondo & Cerrina, 1990; Margaritondo, 1992; Capasso *et al.*, 1993). The positive results of these tests provided the background for more systematic studies like the present one.

Our experiments were conducted with the XSEM photoelectron spectromicroscopy technique (Tonner & Harp, 1988; Koranda & Zhang, 1992). In essence, monochromatized X-ray photons emitted by a synchrotron source (in our case Aladdin at the Wisconsin Synchrotron Radiation Center) stimulate the emission of secondary photoelectrons through intermediate energy-loss steps. It has been demonstrated (Gudat & Kunz, 1972) that intensity *versus* photon energy spectra taken in this way correspond to the X-ray optical absorption coefficient, detected with intermediate surface sensitivity (because of the low energy of the secondary photoelectrons). In the case of XSEM, an electron-optics system is used to process the secondary photoelectrons, to image the geometric features of the specimen and to take spectra on microscopic areas.

The XSEM signal level is sufficient to take real-time video microimages, which can be used for a relatively fast analysis of large portions of the specimen. In our case, this made it possible to analyse several hundred thousand cells over an experimental period of the order of months. Digital subtraction image processing can be routinely used to enhance the signal from a specific element, revealing its spatial distribution.

Parallel tests were systematically performed to assess the possible presence of problems, such as radiation damage or charging, with negative results. We are, therefore, confident that our present results are immune from such problems. Specifically, samples exposed for hours to the monochromatized X-ray beam (whose size was $\sim 0.3 \times 0.3 \text{ mm}^2$) did not exhibit any detectable evidence of damage such as spectral changes. Substantial damage was observed instead after several minutes of exposure to a much more intense unmonochromatized beam (which was never used in our present experiments).

It should be noted that this kind of spectromicroscopy can investigate biological specimens without previous coating and labelling, and therefore, in a state more similar to the natural one than in most electron microscopies. However, this approach is not feasible for the use of live specimens because of the need of an ultra-high vacuum and, therefore, of previous dehydration of the sample.

2.2. Specimen preparation

A detailed description of our specimen preparation process can be found in De Stasio, Perfetti *et al.* (1992)

and De Stasio, Hardcastle *et al.* (1993). In short, granule cells extracted from rat cerebellum were allowed to grow for 8 d on gold substrates. Then, they were washed and exposed for 20 min to a 5 mM solution of either AlF_3 , FeCl_3 or CrCl_2 in uptake buffer. The exposure process included, in some cases, the use of excitatory amino acids, either kainate or glutamate which, however, produced no noticeable differences in the uptake process.

After carefully washing to remove all the residual metal, the metal that had been uptaken was induced to precipitate as a sulfide. After further washing, the cultures were fixed with *p*-formaldehyde and dehydrated.

The specimen analysis prior to the photoelectron spectromicroscopy studies involved optical microscopy, viability tests and induced coupled plasma atomic emission spectroscopy (ICP-AES) for quantitative analysis of the toxic elements (De Stasio, Perfetti *et al.*, 1992; Alimonti, Caroli, Musmeci, Piccioni & Ziemacki, 1988; Sabbioni *et al.*, 1990). The ICP-AES results for samples prepared exactly as for the XSEM experiments are discussed at length by De Stasio, Perfetti *et al.* (1992); specifically, the results for aluminium-exposed granule-cell specimens revealed negligible amounts of aluminium, consistent with the XSEM results. Viability tests were performed with the 3-(4,5-dimethylthiazol-2-yl)-2,5-diphenyltetrazolium bromide (MTT) method (Hansen, Nielsen & Berg, 1989) only after aluminium exposure, and demonstrated a cell survival of the order of 95% or more.

A control experiment was performed on a specimen not exposed to any metal in the uptake buffer, showing no evidence for any of the metals investigated here.

3. Results and discussion

3.1. Aluminium-exposed specimens

Analysis of the aluminium distribution was extended to several specimens; from the average neuron cell density and from the total specimen area, we estimate that the analysis was performed on a total number of cells of approximately 10^5 . The digital subtraction technique enabled us to detect the presence of aluminium rapidly, thereby making it possible to exclude its presence in a large number of cells almost in real time. Spectroscopic evidence for the presence of aluminium was obtained in three specific microscopic sample areas.

XSEM was used to investigate the morphological characteristics of the sample areas that contained aluminium. An example of this analysis is shown in Fig. 1. Specifically, the top two parts of Fig. 1 show XSEM microimages of the same general area, taken with two different magnifications. The aluminium distribution was revealed by taking images at photon energies below and above the Al $2p$ absorption threshold (74 and 78 eV); the digital intensity subtraction of these two images provided the aluminium distribution map.

This map is shown in black in the bottom part of Fig. 1, superimposed for reference on an intensity-reduced, edge-

enhanced version of the centre image of the same figure. It is clear that aluminium is very localized, as confirmed by the spectra of Fig. 2. These two spectra were taken simultaneously from the correspondingly labelled microscopic areas of the central image in Fig. 1, one on the cell body (a) and the other (b) on a cell structure, probably a

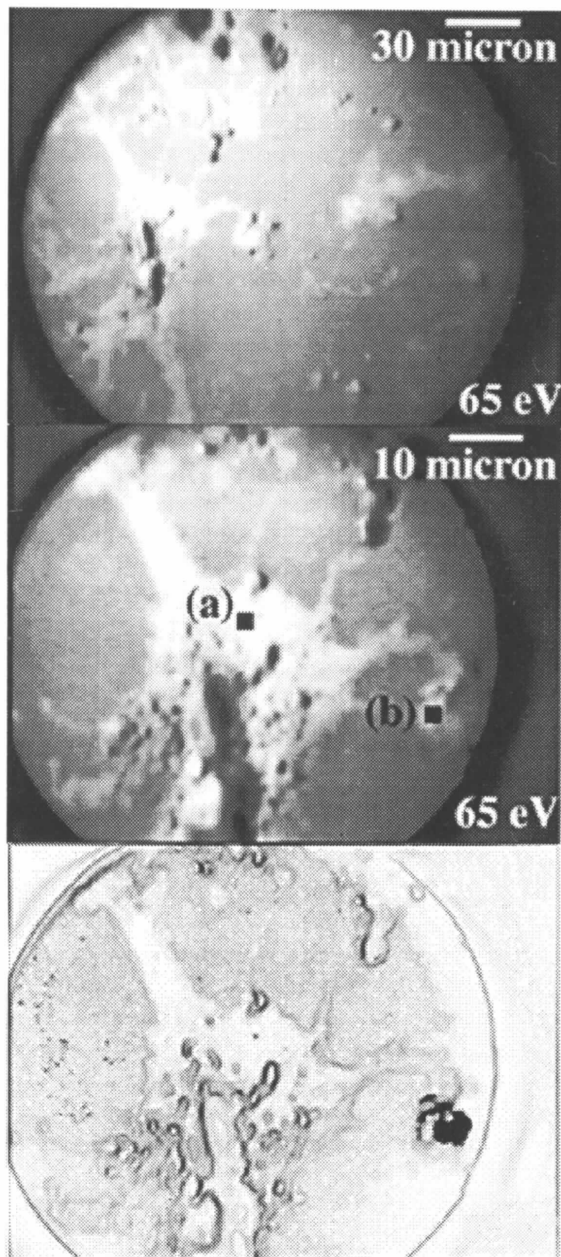


Figure 1

Top and center: XSEM micro-images of the same general area, obtained by detecting secondary photoelectrons, at a photon energy of 65 eV, taken with two different magnifications. The labels in the central image refer to the spectra in Fig. 2. Bottom: the background is shown for reference and it is a low-intensity, edge-enhanced version of the centre image of the figure. The aluminium spatial distribution map is shown superimposed in black on the reference image. This distribution map was obtained by digitally subtracting from an image taken at 78 eV (above the Al $2p$ edge) an image of the same area taken at 74 eV (below the edge).

growth cone. The aluminium edge is clearly visible in (b) and absent from spectrum (a).

The double-test approach based on the parallel use of the digital image subtraction technique and of spectra from selected microscopic areas was used throughout the investigations. Data like those of Figs. 1 and 2 are representative of an extensive search for aluminium conducted on the $\sim 10^5$ cell specimens. Evidence for aluminium was found for only two other cells besides that of Fig. 1.

The morphological characteristics of all of the aluminium-containing cells were carefully examined. First of all, their morphology appears different from that of the granule cells that form the rest of the cultures. Specifically, granule cells have almost round cell bodies whose dimensions are $\sim 5\text{--}8\ \mu\text{m}$, and typically have less than five neurites departing from a body; the aluminium-containing cells have much larger cell bodies ($30\text{--}40\ \mu\text{m}$) and many more fine structures. As is evident from Fig. 1, these morphological characteristics are consistent with the cell's identification as a glial cell or a Purkinje neuron (Cohen-Cory, Dreyfus & Black, 1991; Reynolds & Wilkin, 1988; Linden, Dickinson, Smeyne, Sun & Connor, 1992, and references therein). The same conclusion is valid for the two other cells in which aluminium was found, although the morphological analysis was complicated for one of them by the high density of the surrounding granule cells.

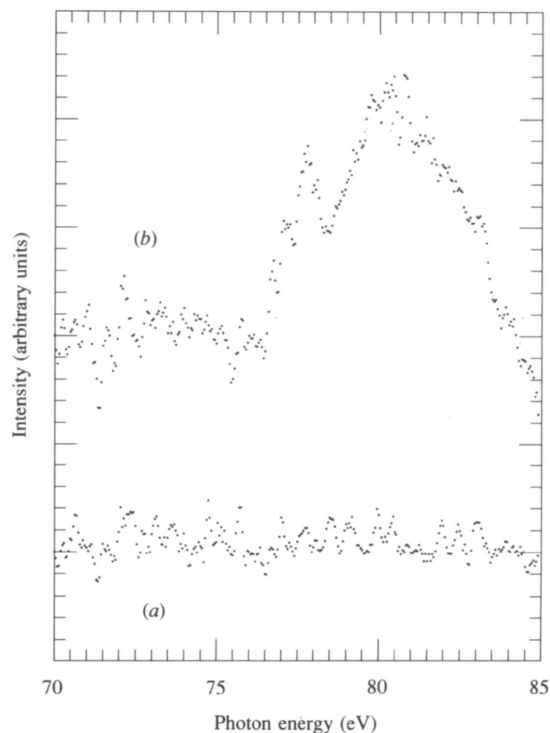


Figure 2

XSEM spectra simultaneously taken in the two microscopic areas labelled as (a) and (b) in the center of Fig. 1, corresponding to (a) the cell body of a Purkinje neuron (or glial cell), and (b) a smaller morphological feature, probably a growth cone. Curve (b) exhibits the Al $2p$ optical absorption edge, whereas no edge is visible for curve (a).

We note that *no other* glial cells or Purkinje neurons were found in the two specimens, consistent with their scarcity in granule-cell cultures (Levi *et al.*, 1989).*

Even conservatively assuming that only two of the three aluminium-containing cells can be definitely identified as non-granule cells in the two specimens, a simple statistical analysis shows that the probability of our event (aluminium in the two non-granule cells and in one granule cell) under the hypothesis of a random distribution would be $\sim 10^{-9}$.

We believe, therefore, that our findings have sufficient statistical significance to suggest a correlation between non-granule cells and aluminium uptake.

* We note that the overall number of Purkinje cells or glial cells in cultures of this type is much less than 1%. Furthermore, an even smaller fraction is visible in our XSEM experiment, since most of the glial subpopulation consists of type I glial cells which are flat and lie underneath granule-cell clusters. From our empirical observations in cultures of this type, we therefore estimate that the visible fraction would not exceed 0.01% of the total population.

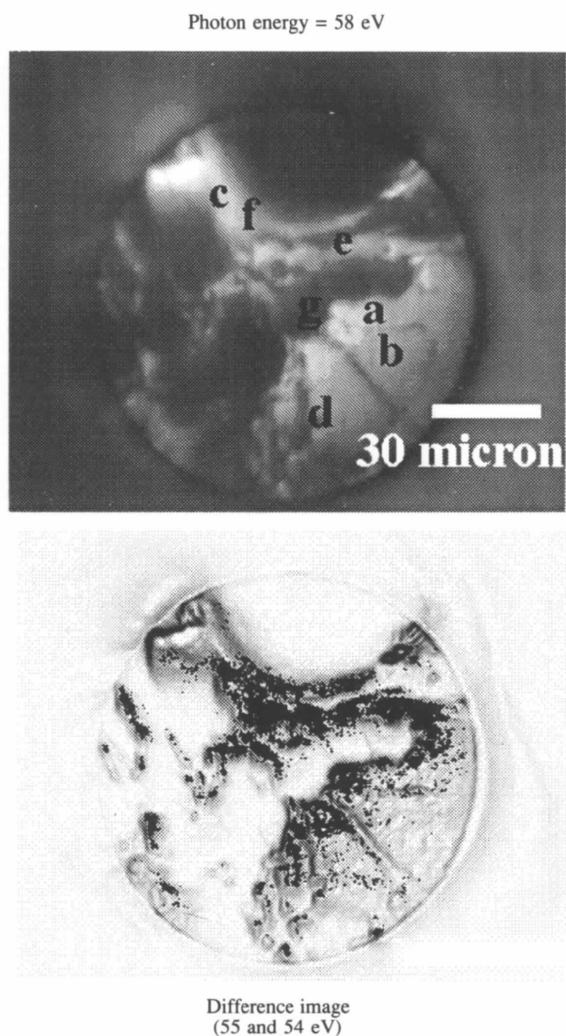


Figure 3

Top: XSEM microimage of a portion of an iron-exposed neuron culture, obtained at a photon energy of 58 eV. The labels refer to the spectra in Fig. 4. Bottom: iron distribution map obtained by digitally subtracting 55 and 54 eV images, superimposed on a low-intensity reference image.

3.2. Iron-exposed specimens

Figs. 3–5 illustrate some of the results obtained on iron-exposed specimens. The XSEM micrograph in the top part of Fig. 3 shows the overall morphology of a portion of a specimen; the small letters indicate the microscopic areas from which XSEM spectra were taken. The bottom part of the same figure is a digital subtraction micrograph obtained from images taken at photon energies near the Fe 3*p* edge (55 and 54 eV) corresponding to strong and weak iron absorption.

It is quite clear that the localization is much more limited than for aluminium. Most of the detected iron is in substrate areas, whereas no aluminium was detected in the substrate areas of the aluminium-exposed samples. Some accumulation of iron, however, is found in cell areas, but it is not primarily limited to non-granule cells as for aluminium.

Fig. 4 shows XSEM spectra simultaneously taken in the microscopic areas correspondingly labelled in the top part of Fig. 3. The rough spectral position of the iron absorption features can be seen in the curve labelled as (s) which was taken on the stainless steel sample holder. The correspondence between the spectroscopic features of the stainless steel spectrum and those of the other spectra is evident. However, the relative weight of each feature can change from spectrum to spectrum: this is particularly evident for the lower photon-energy feature which is quite weak in some parts of the spectra and strong in others [*e.g.* spectrum (g)].

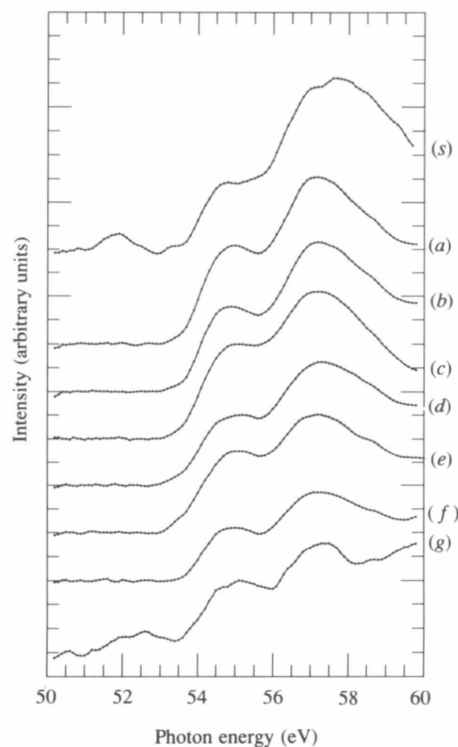


Figure 4

XSEM local spectra from microscopic areas labelled as (a) to (g) in the upper part of Fig. 3. Curve (s) is a reference Fe 3*p* edge spectrum from the stainless steel sample holder.

Spectra (a)–(f) were taken from substrate areas, whereas spectrum (g) is representative of the results from cell-occupied areas. A series of spectra of this latter kind reveal substantial variations in the relative weight of the different spectral features, providing nonetheless, clear evidence of iron presence.

We also used the iron-exposed specimens for a sensitivity estimate of our spectromicroscopy technique. For such an estimate we choose the P 2*p* edge because phosphorus is ubiquitous and homogeneously distributed in cells, at least on the sub-micrometer scale characteristic of XSEM spectromicroscopy.

First, we took the P 2*p* absorption spectra presented in Fig. 5. The top two spectra were taken on cell bodies and clearly reveal the presence of phosphorus. The P 2*p* signal is much weaker or non-existent in the other four spectra, which were taken on substrate areas. Then we performed a quantitative analysis of phosphorus concentration by ICP-AES, a very sensitive technique for chemical analysis (De Stasio, Perfetti *et al.*, 1992; Alimonti, Caroli, Musmeci, Piccioni & Ziemacki, 1988; Sabbioni *et al.*, 1990).

The ICP-AES results demonstrated an average concentration of phosphorus of approximately $0.8 \mu\text{g ml}^{-1}$ when 1.2×10^6 cells were suspended in 1 ml of HNO_3 . This number of cells occupy a volume of $1 \mu\text{l}$, thus *in the cells*, there was a phosphorus concentration of $0.8 \mu\text{g } \mu\text{l}^{-1}$. The

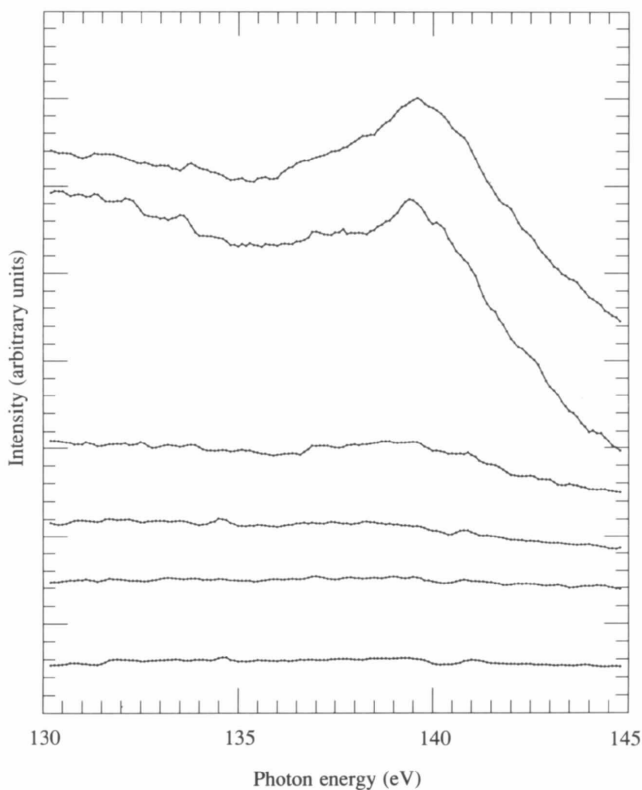


Figure 5
XSEM local spectra from microscopic areas of an iron-exposed specimen, showing the spectral range of the P 2*p* edge. The two top curves reveal naturally present phosphorus.

photoelectron spectromicroscopy signal was clearly visible. From its noise level, we estimate that a signal at least one order of magnitude smaller could be detected. Therefore, we conclude that the sensitivity of photoelectron spectromicroscopy in detecting phosphorus is of the order of at least 80 p.p.m. The sensitivity to other elements depends, of course, on the absorption cross section of the specific core edge.

3.3. Chromium-exposed specimen

Figs. 6 and 7 illustrate some of the results obtained for chromium-exposed specimens, in the form again of micrographs, digital-subtraction images and simultaneously taken spectra from microscopic areas. The latter spectra clearly reveal the presence of chromium and its inhomogeneous distribution; note, in particular, the characteristic white lines of the Cr 2*p* absorption edge.

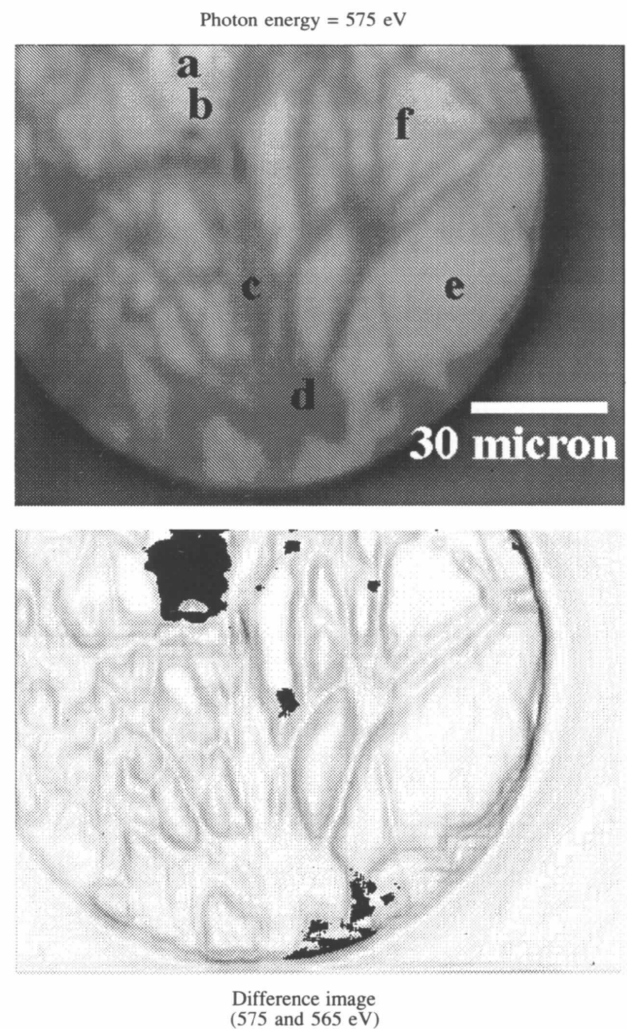


Figure 6
Top: XSEM microimages of a portion of a chromium-exposed neuron culture, obtained at a photon energy of 575 eV. The labels refer to the spectra in Fig. 7. Bottom: reference image and chromium distribution map obtained by digitally subtracting 575 and 565 eV images.

The digital-subtraction image of Fig. 6 (bottom) illustrates yet another type of spatial distribution, different with respect to both aluminium and iron. Chromium is not spread to large areas of the specimen, but localized to areas less than $\sim 20\ \mu\text{m}$ wide. Contrary to the case of aluminium, however, the localization is not confined to cells: each chromium-containing patch belongs in part to the substrate and in part to cell structures.

The inhomogeneity of the chromium distribution, already clear in Fig. 6, is all the more evident when the analysis is extended to the spectra of Fig. 7, corresponding to the labelled areas of Fig. 6 (top). The sharp white-line peaks from chromium are in fact quite intense for the two spectra, and much weaker but still visible for the other curves. Note that the weak chromium signal in these curves does not correspond to evidence of chromium in the (bottom) digital-subtraction image of Fig. 6. This can be explained in two possible ways. First, there is a difference in sensitivity between the two techniques, therefore the spectra might be capable of revealing smaller amounts of chromium than the digital-subtraction images. On the other hand, the XSEM instrument is affected by some defocusing of the electron beams; this could introduce a spurious signal originating from areas surrounding the analysed one. These problems were analysed by tests on non-biological systems, specifically patterned gold on chromium; we found that the corresponding spurious background extends no more than $5\ \mu\text{m}$ beyond the real features and its intensity does not exceed 2% of the signal from real features.

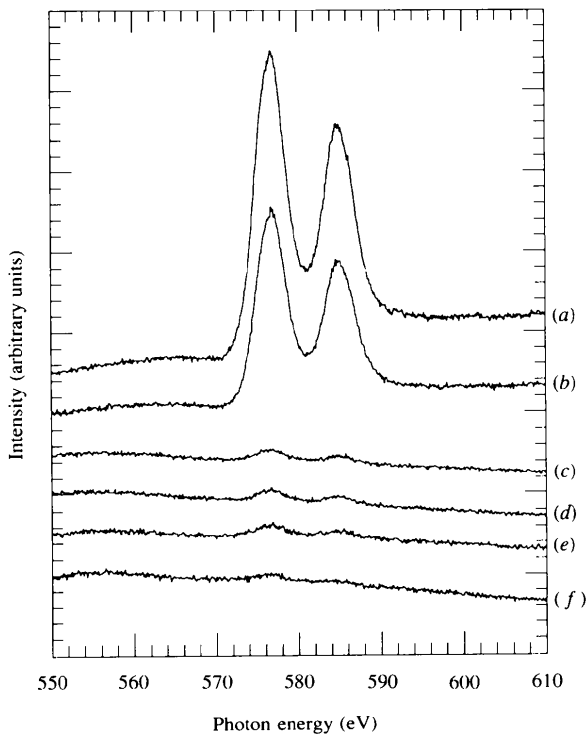


Figure 7
XSEM Cr 2p local spectra from microscopic areas labelled (a) to (f) in the upper part of Fig. 6.

4. Conclusions

Systematic studies of the distribution of artificially added or naturally present elements were performed on a series of fixed and dehydrated but unstained, unlabelled and uncoated neuron specimens using the XSEM version of synchrotron-radiation photoelectron spectromicroscopy. The results show evidence of the presence of the four investigated elements, aluminium, iron, chromium and phosphorus. They also provide evidence that the space distribution is highly inhomogeneous for the added elements. Furthermore, the qualitative characteristics of the distribution markedly change from element to element.

We also demonstrated that the sensitivity of photoelectron spectromicroscopy in detecting phosphorus is of the order of at least 80 p.p.m.

In the case of iron and chromium, we not only found the toxic element in biological structures, but also on the substrates. Iron was spread through large portions of the specimens, whereas chromium was much more localized, and confined to patches.

The most interesting results were obtained in the case of aluminium, whose signal was found only on biological structures. Moreover, the morphological analysis indicates that all of the cells active in aluminium uptake are of the same type, which is quite rare for these kind of cultures: Purkinje neurons or glial cells (Cohen-Cory, Dreyfus & Black, 1991; Reynolds & Wilkin, 1988; Linden, Dickinson, Smeyne, Sun & Connor, 1992, and references therein; Levi *et al.*, 1989).

This conclusion is fully consistent with Zatta's results (Favarato, Zatta, Perazzolo, Fontana & Nicolini, 1992; Zatta & Favarato, 1993) obtained with fluorescence microscopy. Zatta's results and ours are, of course, steps following many previous studies (Candy *et al.*, 1992; Chafi, Hauw, Rancurel, Berry & Galle, 1991; Connick *et al.*, 1991; Takeda *et al.*, 1991; Farrar *et al.*, 1990; Lugowski, Smith, McHugh & Van Loon, 1991; Perl & Brody, 1980; Perl, Gadjusek, Garruto, Yanagihara & Gibbs, 1982) of aluminium in neurons that identified, for example, aluminium in human brains (Candy *et al.*, 1992) and found a correlation between aluminium and human pathologies such as the Alzheimer and Parkinson diseases (Perl & Brody, 1980; Perl, Gadjusek, Garruto, Yanagihara & Gibbs, 1982).

Very recently, additional evidence of the special role played by non-granule cells in aluminium uptake was corroborated by results on homogeneous Purkinje or glial cell cultures. In such cultures, almost all cells took up aluminium.

This work was supported by the Fonds National Suisse de la Recherche Scientifique, the Consiglio Nazionale delle Ricerche, the US National Science Foundation and the EPFL, and performed at the Wisconsin Synchrotron Radiation Centre, a national facility supported by the NSF. We thank Carlo Coluzza, Mario Capozzi, Sandro

Rinaldi, Bruno Nicolini, Marino Marsi and Tiziana dell'Orto for their expert help, and Paolo Zatta and Maddalena Pedio for stimulating discussions.

References

- Alimonti, A., Caroli, S., Musmeci, L., Piccioni, A. & Ziemacki, G. (1988). *Sci. Total Environ.* **71**, 495–499.
- Candy, J. M., Oakley, A. E., Mountfort, S. M., Taylor, G. A., Morris, C. M., Bishop, H. E. & Edwardson, J. A. (1992). *Biol. Cell.* **74**, 109–207.
- Capasso, C., Ng, W., Ray-Chaudhuri, A. K., Liang, S. H., Cole, R. K., Guo, Z. Y., Wallace, J., Cerrina, F., Underwood, J., Perera, R., Kortright, J., De Stasio, G. & Margaritondo, G. (1993). *Surf. Sci.* **287/288**, 1046–1050.
- Chafi, A. H., Hauw, J.-J., Rancurel, G., Berry, J. P. & Galle, C. (1991). *Neurosci. Lett.* **123**, 61–64.
- Cohen-Cory, S., Dreyfus, C. F. & Black, I. B. (1991). *J. Neurosci.* **11**, 462–468.
- Connick, J. H., Lombardi, G., Moroni, F., Hall, E., Taylor, A. & Stone, T. W. (1991). *Kyurenine and Serotonine Pathways*, edited by R. Schwarcz *et al.*, pp. 459–463. New York: Plenum Press.
- De Stasio, G., Capasso, C., Ng, W., Ray-Chaudhuri, A. K., Liang, S. H., Cole, R. K., Guo, Z. Y., Wallace, J., Cerrina, F., Margaritondo, G., Underwood, J., Perera, R., Kortright, J., Mercanti, D., Ciotti, M. T. & Stecchi, A. (1991). *Europhys. Lett.* **16**, 411–414.
- De Stasio, G., Cerrina, F., Tonner, B. P., Mercanti, D. & Margaritondo, G. (1994). *Life Chemistry Reports*, edited by P. Zatta. London: Harwood. In the press.
- De Stasio, G., Dunham, D., Tonner, B. P., Mercanti, D., Ciotti, M. T., Perfetti, P. & Margaritondo, G. (1993). *NeuroReport* **3**, 1175–1179.
- De Stasio, G., Hardcastle, S., Koranda, S. F., Tonner, B. P., Mercanti, D., Ciotti, M. T., Perfetti, P. & Margaritondo, G. (1993). *Phys. Rev. E*, **47**, 2117–2121.
- De Stasio, G., Koranda, S. F., Tonner, B. P., Harp, G. R., Mercanti, D., Ciotti, M. T. & Margaritondo, G. (1992). *Europhys. Lett.* **19**, 655–659.
- De Stasio, G., Ng, W., Ray-Chaudhuri, A. K., Cole, R. K., Guo, Z. Y., Wallace, J., Margaritondo, G., Cerrina, F., Underwood, J., Perera, R., Kortright, J., Mercanti, D. & Ciotti, M. T. (1990). *Nucl. Instrum. Methods*, **A294**, 351–354.
- De Stasio, G., Perfetti, P., Ng, W., Ray-Chaudhuri, A. K., Liang, S. H., Singh, S., Cole, R. K., Guo, Z. Y., Wallace, J., Capasso, C., Cerrina, F., Mercanti, D., Ciotti, M. T., Gozzo, F. & Margaritondo, G. (1993). *Phys. Rev. E*, **48**, 1478–1482.
- De Stasio, G., Perfetti, P., Oddo, N., Galli, P., Mercanti, D., Ciotti, M. T., Koranda, S. F., Hardcastle, S., Tonner, B. P. & Margaritondo, G. (1992). *NeuroReport* **3**, 965–969.
- Farrar, G., Altmann, P., Welch, S., Wychrij, O., Ghose, B., Lejeune, J., Corbett, J., Prasher, V. & Blair, J. A. (1990). *Lancet*, **335**, 747–752.
- Favarato, M., Zatta, P., Perazzolo, M., Fontana, L. & Nicolini, M. (1992). *Brain Res.* **569**, 330–334.
- Gudat, W. & Kunz, C. (1992). *Phys. Rev. Lett.* **29**, 169–173.
- Hansen, M. B., Nielsen, S. E. & Berg, K. (1989). *J. Immunol. Methods*, **119**, 203–208.
- Koranda, S. F. & Zhang, J. (1992). *Rev. Sci. Instrum.* **63**, 563–567.
- Levi, G., Aloisi, F., Ciotti, M. T., Thangniipon, W., Kingsbury, A. & Balazs, R. (1989). *A Dissection and Tissue Culture Manual of the Nervous System*, edited by A. Shahar, J. de Vellis, A. Vernadakis & B. Haber, p. 211. New York: Alan R. Liss.
- Linden, D. L., Dickinson, M. H., Smeyne, M., Sun, S. C. & Connor, J. A. (1992). *J. Neurosci.* **12**, 3601–3609.
- Lugowski, S. J., Smith, D. C., McHugh, A. D. & Van Loon, J. C. (1991). *J. Biomed. Mater. Res.* **25**, 1443–1449.
- Margaritondo, G. (1988). *Introduction to Synchrotron Radiation*. New York: Oxford.
- Margaritondo, G. (1992). *Acta Phys. Pol.* **82**, 283–294.
- Margaritondo, G. & Cerrina, F. (1990). *Nucl. Instrum. Methods*, **A291**, 26–35.
- Perl, D. P. & Brody, A. R. (1980). *Science*, **208**, 297–300.
- Perl, D. P., Gadjusek, D. C., Garruto, R. M., Yanagihara, R. T. & Gibbs, C. J. (1982). *Science*, **217**, 1053–1055.
- Reynolds, R. & Wilkin, G. P. (1988). *J. Neurosci. Res.* **20**, 311–320.
- Sabbioni, E., Nicolini, G. R., Pietra, R., Beccaloni, E., Coni, E., Alimonti, A. & Caroli, S. (1990). *Biol. Trace Elem. Res.* **26/27**, 757–766.
- Takeda, M., Nishimura, T., Kudo, T., Tanimukai, S., Gotow, T., Tanabe, H., Miki, T., Nakamura, Y., Niigawa, H., Morita, H., Tanaka, T., Tatebayashi, Y. & Tada, K. (1991). *Gerontology*, **37**, 31–38.
- Tonner, B. P. & Harp, G. R. (1988). *Rev. Sci. Instrum.* **59**, 853–861.
- Zatta, P. & Favarato, M. (1993). *NeuroReport* **4**, 1119–1123.